Analysis of electromagnetic characteristics of the main transformer caused by pantograph-catenary disconnection in high speed train

Jin Wang, Zhongping Yang, Fei Lin*, Junci Cao and Wenzheng Liu

School of Electrical Engineering,
Beijing Jiaotong University,
No. 3 ShangyuanCun, Beijing, 100044, China
E-mail: 11121670@bjtu.edu.cn
E-mail: zhpyang@bjtu.edu.cn
E-mail: flin@bjtu.edu.cn
E-mail: jccao@bjtu.edu.cn
E-mail: wzhliu@bjtu.edu.cn
*Corresponding author

Abstract: With the increasing speed of the high-speed train, the disconnection of pantograph-catenary system becomes more frequent which will lead to DC magnetic bias of the main transformer. A coupled finite element model of pantograph-catenary system and a 3D coupled field-circuit model of the main transformer have been set up to analyse this issue. This paper has analysed the current harmonic, electromagnetic field characteristics and leakage inductance which all cause by DC magnetic bias. Results show that with the rising of DC magnetic bias, the current harmonic and secondary leakage inductance are increasing and the primary leakage inductance is decreasing. Variation rules of electromagnetic field have been summed up in this paper.

Keywords: pantograph-catenary system; PCS; main transformer; DC magnetic bias; coupled field-circuit method; electromagnetic characteristics; leakage inductance; pantograph-catenary disconnection; high speed train.

Reference to this paper should be made as follows: Wang, J., Yang, Z., Lin, F., Cao, J. and Liu, W. (2014) 'Analysis of electromagnetic characteristics of the main transformer caused by pantograph-catenary disconnection in high speed train', *Int. J. Engineering Systems Modelling and Simulation*, Vol. 6, Nos. 1/2, pp.91–106.

Biographical notes: Jin Wang is currently studying for a Masters degree in Electrical Engineering School in Beijing Jiaotong University. Her research direction is high speed train traction drive system.

Zhongping Yang received his PhD from Tokyo University in 2002 and worked in Railway Vehicle Technical Department in Japan Toshiba Company. Currently, he is a Professor of Electrical Engineering School in Beijing Jiaotong University. His major researches interests are in high speed train traction drive system and energy saving technology.

Fei Lin received his PhD from Tsinghua University in 2004 and went to Ohio State University to be a Visiting Scholar from 2009 to 2010. Currently, he is an Associate Professor of Electrical Engineering School in Beijing Jiaotong University. His major researches interests are in power electronics and motor control.

Junci Cao received his PhD in Harbin University of Science and Technology. He is an IEEE TIE member, and an Associate Professor for the School of Electrical Engineering of Beijing Jiaotong University. His major researches interests are in design of special motor and traction motor, comprehensive physical field calculation and application in the motor.

Wenzheng Liu received his Master and PhD in Japan. He joined the Hitachi Group in 2001, engaged in product design and development. Currently, he is a Professor for the School of Electrical Engineering of Beijing Jiaotong University. His major researches are in high-speed and overload electrified railway catenary technology.

1 Introduction

With the development of the railway, the highest running speed of the high speed train which is more than 300 km/h has become so common. For instance, the operation speed of Japanese E5 series and German ICE3 trains has already reached 320 km/h. The French TGV created a record of high speed train in a running speed of 574.8 km/h in Paris. And the highest speed of Chinese CRH380A in the test on December 3, 2010 is as high as 486.1 km/h. And The 500 km/h-test-train has completed at CSR Qingdao SiFang Co., LTD in China.

Unfortunately, as the increasing speed of the train, the oscillation of contact force between pantograph and catenary intensifies seriously (Manabe, 1992; Seo et al., 2005; Liu et al., 2011a), this will cause the status of the pantograph-catenary electrical contact deteriorated seriously and generating of disconnection frequently. The pantograph arc arouse at the same time (Liu et al., 2011b; Bucca et al., 2011). Although some literatures have studied the features of pantograph-catenary system (PCS) using field tests (Collina and Bruni, 2002) and establishment of laboratories, computer simulation is a shortcut to research the interaction between pantograph and catenary (Tibor et al., 1997; Hedayati et al., 2010; Robert and Meshal, 2000) due to the restrictions of physical testing and commissioning, The computer simulation method is intuitive and easy to change the conditions and data. Although some approximate properties, it is a main method to study the pantograph-catenary disconnection of the electrical railway.

The PCS is the input of traction drive system in high-speed train (see Figure 1). Main transformer transforms the high voltage get from the pantograph to appropriate voltage which could be supplied for traction converter and other electric equipment. The high frequency disconnection could bring asymmetry voltage waveform and lead to DC magnetic bias of the main transformer, which will have impact on the output characteristic, harmonic
(Siti et al., 2012), electromagnetic features and leakage inductance. Most literatures have been focused on these issues. The bias of converter transformer in power electronics converter circuit is caused by asymmetric drive signal (Zeng et al., 2007; Mei et al., 2008). The failure of HVDC power transmission systems may arouse DC flux in substation transformer. However, the problem of DC magnetic bias of the main transformer caused by high frequency disconnection has not drew great attention. The Shinkansen 300 series train firstly concerned this issue and set up separate-core and gap-core in the main transformer to lessen the impact of DC magnetic bias. So variations of electromagnetic field characteristics before and after the setting must be different. Field-circuit coupling method (Piriou and Razak, 1998; Jianshe, 1996; Tang et al., 2000) which has combined electromagnetic field with external circuit is an effective to study variations of electromagnetic field characteristics. Most literatures had simple descriptions of magnetic density using some cloud charts (Xuejun and Dan, 2010) but without detailed analysis. DC magnetic bias also raise leakage inductance variations, which will react on the grid-side power factor, primary current, secondary current and THD of DC link voltage of traction converter. So the calculation of leakage inductance variations with DC magnetic bias is necessary. The primary inductance was always not separate from secondary inductance in some literatures (Heinemann and Helfrich, 2000; Chan and Pong, 2006). The flux concept to work out the total leakage inductance is employed, which makes the corresponding calculation complicated (Wang et al., 1999). The energy method of calculating inductance is convenient and effective of calculating the leakage inductance of every winding (Li et al., 2008).

DC magnetic bias will lead to local overheating of the transformer which may jeopardise the winding insulation. At the same time, DC-link voltage ripple of traction converter and output traction force pulsation of traction motor (Lee et al., 2006; Frank, 1995; Spangler, 2002; Nystrom et al., 1988) are both result from variations of output features of the main transformer, which will either constrain the energy feedback and safe operation of high speed train.

Figure 1 Traction drive system in high speed train (see online version for colours)

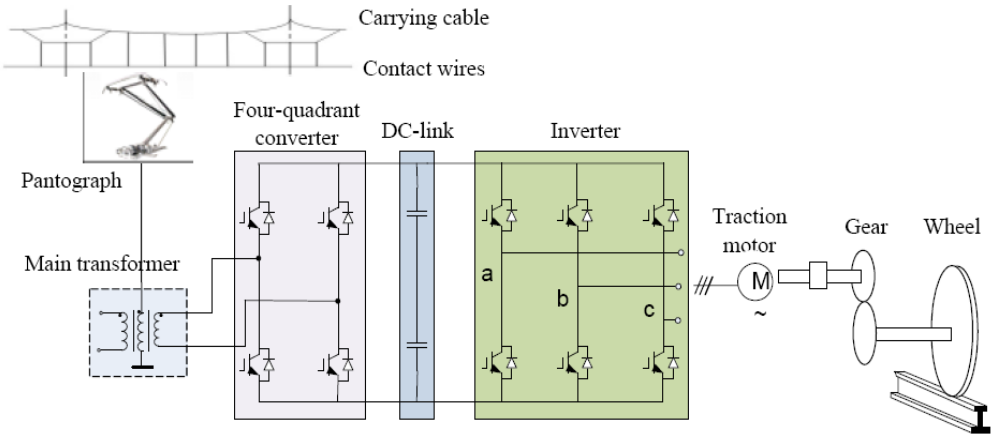

In this paper, coupled finite element model of PCS and coupled field-circuit model of the main transformer have been set up to study DC magnetic bias and other effects of frequent disconnection. This paper has analysed the current harmonic, variation rules of electromagnetic field and leakage inductance which all caused by DC magnetic bias. It is the foundation of further study of bias suppression technology and effects on traction converter and the whole traction drive system caused by disconnection of pantograph.

2 Pantograph-catenary system

2.1 Catenary model

There are many kinds of catenary models in the analysis of the interaction between catenary and pantograph in high speed railway. The most representative models are lumped mass model of Japanese Manabe (Manabe et al., 1986), Euler beam model of American Vinayagalingam (1983) and 'related to frequency model' of German link. The lumped mass model could not express the high frequency vibration of catenary, and regard the carrying cable as Euler beam is imprecision. Combining advantages of these models, the Bernoulli-Euler beam model is used in this paper for catenary.

The motion equations of contact wires can be described as below:

$$m_c \frac{\partial^2 u_c}{\partial t^2} + \frac{\partial^2}{\partial x^2}\left(EI_c \frac{\partial^2 u_c}{\partial x^2}\right) - \frac{\partial}{\partial x}\left(T_c \frac{\partial u_m}{\partial x}\right) + k_d\left(u_m - u_c\right)\delta\left(x - x_n\right) = P\delta(x - Vt) \tag{1}$$

where m_c, EI_c, T_c and k_d express the unit mass, flexural rigidity, tension force and hanger stiffness of contact wires; δ is impact function; P expresses the contact pressure between pantograph and catenary; u_c is the displacement of contact wires; u_m is the displacement of carrying cable; x_n expresses the distance between hanger and motion point; x is the motion point; t is time and V is speed.

The motion equations of carrying cable can be obtained as below:

$$m_m \frac{\partial^2 u_m}{\partial t^2} + \frac{\partial^2}{\partial x^2}\left(EI_m \frac{\partial^2 u_m}{\partial x^2}\right) - \frac{\partial}{\partial x}\left(T_m \frac{\partial u_m}{\partial x}\right) + k_d\left(u_m - u_c\right)\delta\left(x - x_n\right) + k_s u_m\left(s - x_s\right) = 0 \tag{2}$$

where m_m, EI_m, and T_m express the unit mass, flexural rigidity, tension force and hanger stiffness of carrying cable; k_s is the equivalent stiffness of support device, x_s expresses the distance between support point and motion point; x is displacement of the motion point.

2.2 Pantograph model

The pantograph model is a nonlinear model, the motion differential equation can be expressed as:

$$M_H \Delta\ddot{Z}_H + U_H\left(\Delta\dot{Z}_H - \Delta\dot{Z}_E\right) + B_H \sin\left(\Delta\dot{Z}_H - \Delta\dot{Z}_E\right) + K_H\left(\Delta\dot{Z}_H - \Delta\dot{Z}_E\right) = F_{c0} - F_c \tag{3}$$

where M_H, U_H, B_H and K_H express the mass, damping, dry friction and stiffness of pantograph bow; F_{c0} and F_c express the static contact pressure and dynamic contact pressure relatively.

The pantograph model consists of three main parts: main frame, lower frame and pushrod, pantograph head and pantograph pan. All three parts are linked by hinge connection and nonlinear springs. Relative rotation of hinges in coordinates of x direction is allowed. Moreover, the high frequency vibration of pantograph head and pantograph slide plate are considered in the model. Figure 2 shows the coupling model of PCS.

Figure 2 PCS model (see online version for colours)

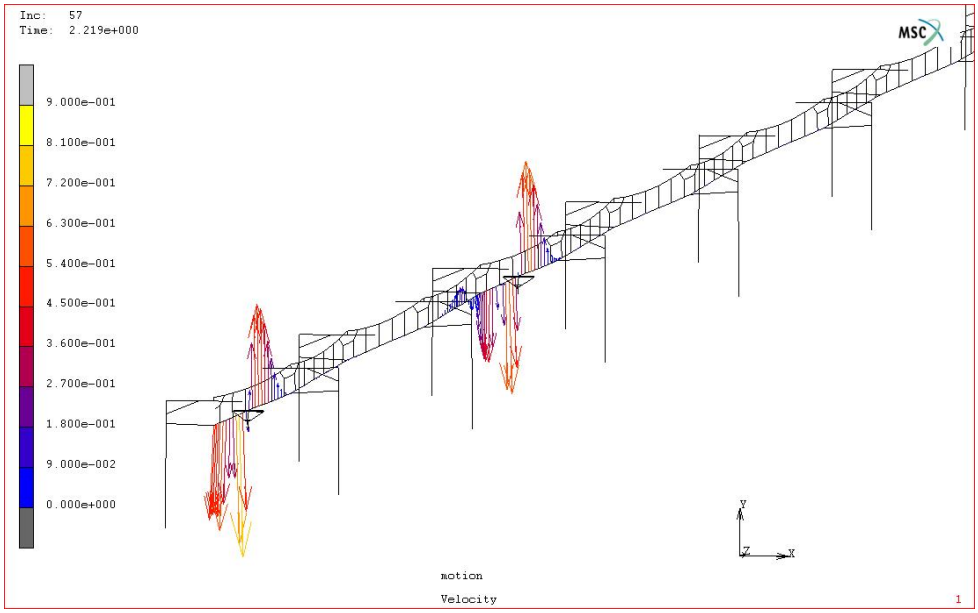

The pantograph-catenary finite element model is modelled by MSC. Marc software. The catenary model of six span lengths and seven poles is composed of contact wires, carrying cables, stitch wires, droppers, poles. And carrying cables and contact wires are both taking into account the elastic and damping. Table 1 shows the basic parameters of the catenary.

Table 1 Basic parameters of the catenary

Items	*Parameters*
Span number	24
Span length/m	50
System height/mm	1,600
Carrying cable tension/kN	21
Contact line tension/kN	30

2.3 Disconnection rules of PCS

Take the case of 400 km/h as an example, Figure 3(a) shows the contact pressure curve between pantograph and catenary. Regard contact pressure larger than 0 as good contact and equal to 0 as disconnection. Corresponding disconnection rules could be obtained from Figure 3(b), sign '1' expresses good contact and sigh '0' expresses disconnection. During 1.8 s to 4.5 s, ten parts of disconnection were shown in Figure 3(b), among them, time of C part is the longest (0.11s) and time of F, G and H are shortest (0.03 s).

3 The main transformer

3.1 Field-circuit coupled model

In the problems of practical electromagnetic field, as the voltage and current sources are non sinusoidal, the magnetic field, energy, force are all functions of time. Transient analysis is necessary in this situation. According to the basic Maxwell equations, we can obtain the following equation:

$$\nabla \times H = J_s - \sigma \frac{\partial A}{\partial t} \tag{4}$$

where H, J_s, σ and $\sigma \partial A/\partial t$ express the magnetic force, current density, conductivity of the material and eddy current density respectively.

Ignore the hysteresis effect of ferromagnetic material, and then:

$$H = \frac{1}{\mu} B = \frac{1}{\mu} \nabla \times A \tag{5}$$

where μ expresses the magnetic permeability and B express the magnetic flux density.

According to equation (4) and (5), we can obtain the following equation (6):

$$\nabla \times \frac{1}{\mu} (\nabla \times A) = J_s - \sigma \frac{\partial A}{\partial t} \tag{6}$$

And equation (6) could be expressed as equation (7):

$$\begin{aligned} &\frac{\partial}{\partial x}\left(\frac{1}{\mu_x}\frac{\partial A}{\partial x}\right) + \frac{\partial}{\partial y}\left(\frac{1}{\mu_y}\frac{\partial A}{\partial y}\right) \\ &+ \frac{\partial}{\partial z}\left(\frac{1}{\mu_z}\frac{\partial A}{\partial z}\right) - J_s + \sigma \frac{\partial A}{\partial t} = 0 \end{aligned} \tag{7}$$

Equation (7) can be weighed-integral discrete as the following one:

$$[K]\{A\} + [M]\frac{\partial}{\partial t}\{A\} - [C]\{I\} = 0 \tag{8}$$

where K and M are related to the coefficient matrix and element type relatively. And C expresses the interaction with current and cell node.

Figure 3 Contact pressure curve (see online version for colours)

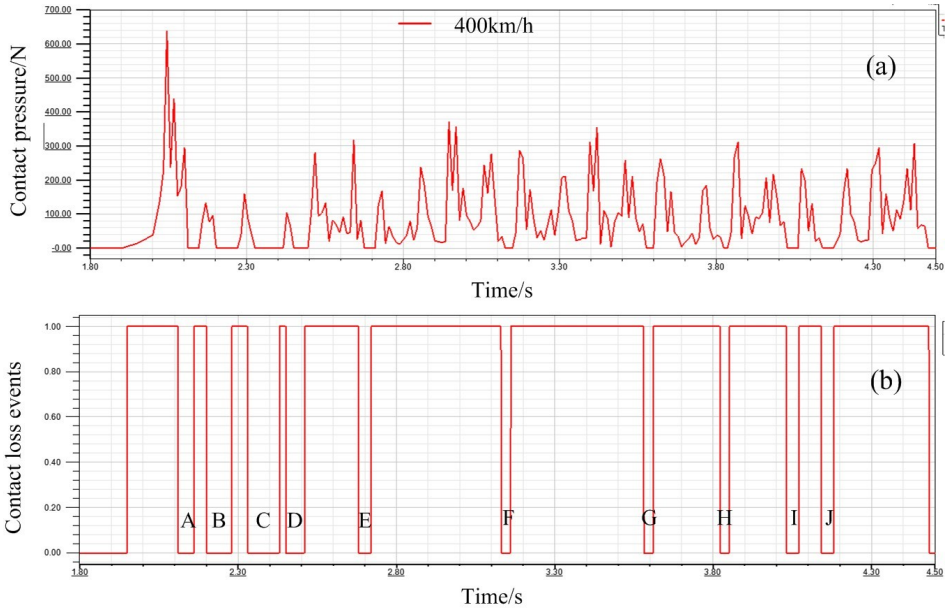

The excitation of this model is voltage source, and the external circuit equation can be described as follow:

$$\{U\} = \{E\} - [R]\{i\} - [L]\frac{\partial\{i\}}{\partial t} \tag{9}$$

where $\{U\}$, $\{i\}$, $\{E\}$, $[R]$ and $[L]$ express the exciting voltage, winding current, induced electromotive force, external resistance and external inductance relatively.

The induced electromotive force could be expressed as:

$$E = \frac{n}{S}\frac{\partial}{\partial t}\int_{\Omega} A \bullet l d\Omega \tag{10}$$

where l is the tangential unit vector of the winding.

According to the equation (9) and (10), the external circuit equation of transformer can be expressed as:

$$\{U\} = \frac{n}{S}\frac{\partial}{\partial t}\int_{\Omega} A \bullet l d\Omega - [R]\{i\} - [L]\frac{\partial\{i\}}{\partial t} \tag{11}$$

The matrix equation of equation (11) can be written as follow:

$$[C]^T \frac{\partial}{\partial t}\{A\} - [R]\{i\} - [L]\frac{\partial}{\partial t}\{i\} = \{U\} \tag{12}$$

Combine equation (8) and equation (12), a matrix equation of coupled field-circuit mathematical model can be expressed as below:

$$\begin{bmatrix} K & -C \\ 0 & R \end{bmatrix}\begin{Bmatrix} A \\ I \end{Bmatrix} + \begin{bmatrix} M & 0 \\ C^T & L \end{bmatrix}\frac{d}{dt}\begin{Bmatrix} A \\ I \end{Bmatrix} = \begin{Bmatrix} 0 \\ U \end{Bmatrix} \tag{13}$$

Coupled field-circuit model of the main transformer can be set up according to the equation (13).

The strength of the magnetic field can be expressed as magnetic density B (Mag_B). The vector magnetic potential A in every node could be received from the coupled field-circuit method, and the relationship between Mag_B and A can be expressed as:

$$B = \nabla \times A = x_e \frac{\partial A}{\partial x} + y_e \frac{\partial A}{\partial y} \tag{14}$$

The leakage field energy consists of two main parts: energy in windings and energy in gaps. Both of them can be described as:

$$W_\sigma = \frac{1}{2}\int_V B \bullet H dV \tag{15}$$

And leakage inductance can be described as follow:

$$L_\sigma = \frac{2W_\sigma}{I^2} \tag{16}$$

According to equations (14) to (16), Mag_B, leakage field energy and leakage inductance can be received by post processing.

3.2 Electromagnetic field model

According to the winding arrangement and equal impedance voltage of CRH2 EMU in China, a shell-type transformer is designed (two primary windings with parallel connection and two secondary windings). Table 2 presents basis parameters.

Table 2 Main technical parameters of transformer

Items	*Parameters*
Capacity/kVA	15
Rated voltage/V	220/220 × 2
Rated current/A	68/34 × 2
Frequency/Hz	50
Phase	Single
Winding material	Aluminium
Core material	DW310-35
Core LWH/mm	320/180/240
Window LWH/mm	80/180/160
Turns	63/63/63/63
Windings LWH/mm	75/340/6
Temperature/□	<70

The structure and electromagnetic distribution features of the main transformer are symmetry. So we set up a 1/4 model of transformer. This model had neglect impact on magnetic field of core eddy current, winding circulation and hysteresis effect. Boundary conditions are zero tangential H field and symmetry. The model should be minuteness meshed because of magnetic meticulous solution. So core is meshed into four layers, windings are meshed into two layers, which is more meticulous than core mesh plot in Figure 4(a). Figure 4(b) shows the flux density vector.

4 Results and discussion

4.1 DC magnetic bias and current

Disconnection rules in Figure 3(b) could be regarded as control sign of input voltage of transformer, and the external circuit model could emulate with electromagnetic field model based on coupled field-circuit method.

Figure 5 shows simulation results. Flux will decrease slowly after the input voltage changes to 0 suddenly. If the pantograph gets contact with catenary next time, flux may not reduce to 0 during the disconnection time. This is the so-called remanence in the core. Moreover, an aperiodic component will appear at the moment of reconnection of PCS unless the pantograph voltage phase is $\pi/2$. The aperiodic component is exponential decreasing. So high frequency disconnection will arouse the superposition of remanence and aperiodic flux component.

Figure 4 Mesh plot and B vector (see online version for colours)

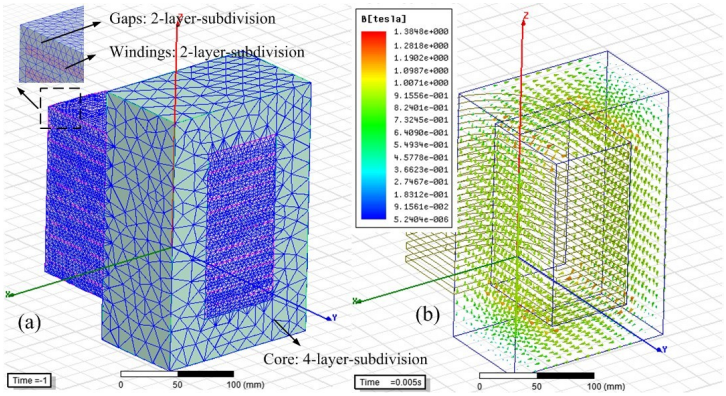

Figure 5 Flux and primary current (see online version for colours)

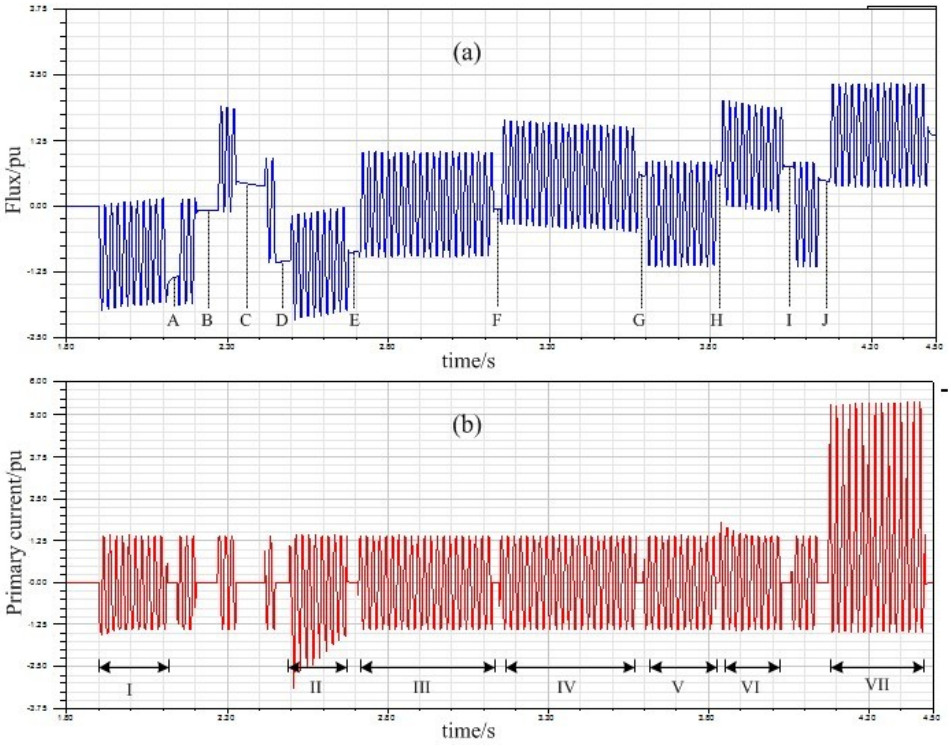

In Figure 5(a), C, E, F, G and I can be summarised that the orientation of remanence and aperiodic component is opposite, so the DC magnetic bias will be receded and lead to slight core saturation, and amplitude change of primary current is not obvious (see III, IV, V). For A, B, D, H and G, remanence and aperiodic component is in same direction, which make core saturation aggravate and DC component in primary current is increasing sharply (see II, VI, VII). Distortion becomes more serious at the same time. The reason is that the relative permeability and excitation inductance will be rapid decrease as the deep core saturation. But the secondary current (not display in Figure 5) almost does not change because of the DC blocking of transformer.

Table 3 shows the harmonic of part I, II, IV, VI and VII of primary current in Figure 5. From Table 3, with the rising of DC magnetic bias, there is not only odd harmonic but also even harmonic. These sections show in Table 3 can be ranged as that 'IV < I < VI < II < VII' based on the extent of core saturation. So the harmonic content is increasing no matter odd or even with the intensified core saturation.

Table 3 Harmonic analysis of primary current

Items	*DC/pu*	*Harmonic (%)*			
		2nd	*3rd*	*4th*	*5th*
I	0.171	13.7	8.1	3.63	0.95
II	0.409	31.61	17.75	7.85	3.12
IV	0.0001	0.00	0.03	0.02	0.04
VI	0.188	17.26	9.9	4.18	0.96
VII	1.03	49.27	24.63	8.95	1.98

4.2 Electromagnetic field of core

Figure 6 shows the Mag_B and magnetic lines of the main transformer of 2D model. From Figure 6(b), it can be seen that the magnetic line looks like several rounded rectangles. So magnetic lines at the edge and middle of iron yoke are thin which of other parts [see rectangular box 1, 2, 3 and 4 in Figure 6(a)], and the Mag_B of these rectangular boxes is less. Instead, magnetic lines gathered together inside the corner of core which is the most intensive position [see circle 5, 6, 7 and 8 in Figure 6(a)]. So Mag_B in the circle 5, 6, 7 and 8 is the largest.

In order to study internal electromagnetic field features of core, it is necessary to print four lines in xz coordinate section to analyse Mag_B of some special nodes on these lines. Horizontal lines sign 'core_up' and 'core_max' relatively in the iron yoke, which have several nodes of 'Ai' and 'Mi'. Vertical lines sign 'core_centre' and 'core_right' in the centre column of core and the iron yoke relatively, which have nodes of 'Bi' and 'Ci' (Figure 6). And every line follows the drawing principle of 'from left to right' and 'from top to bottom'. Take line 'core_up' as an example, its starting point is A1 at the far left, go through A2,…, A5, and reach A6 point at the right end of the line. In a similar way, 'core_right' line is draw from top to bottom which go through C1, C2 and C3 point in sequence.

According to the coupled field-circuit simulation results, different DC magnetic bias value could be obtained from Figure 5. We pick out eight values of DC flux from 0 pu to 1.008 pu to get the maximum of Mag_B(T) at different nodes in Figure 8. And some special nodes have been marked in Figures 7 and 8. The horizontal ordinate of Figure 8 is length (mm) of lines; the coordinate zero '0 mm' of horizontal ordinate expresses the start node at the far left or the top of lines, and the coordinate end of horizontal ordinate expresses the finishing node at the far right or the bottom of lines. The vertical ordinate is the maximum of Mag_B(T) of different DC flux.

Figure 6 Cloud picture of 2D (see online version for colours)

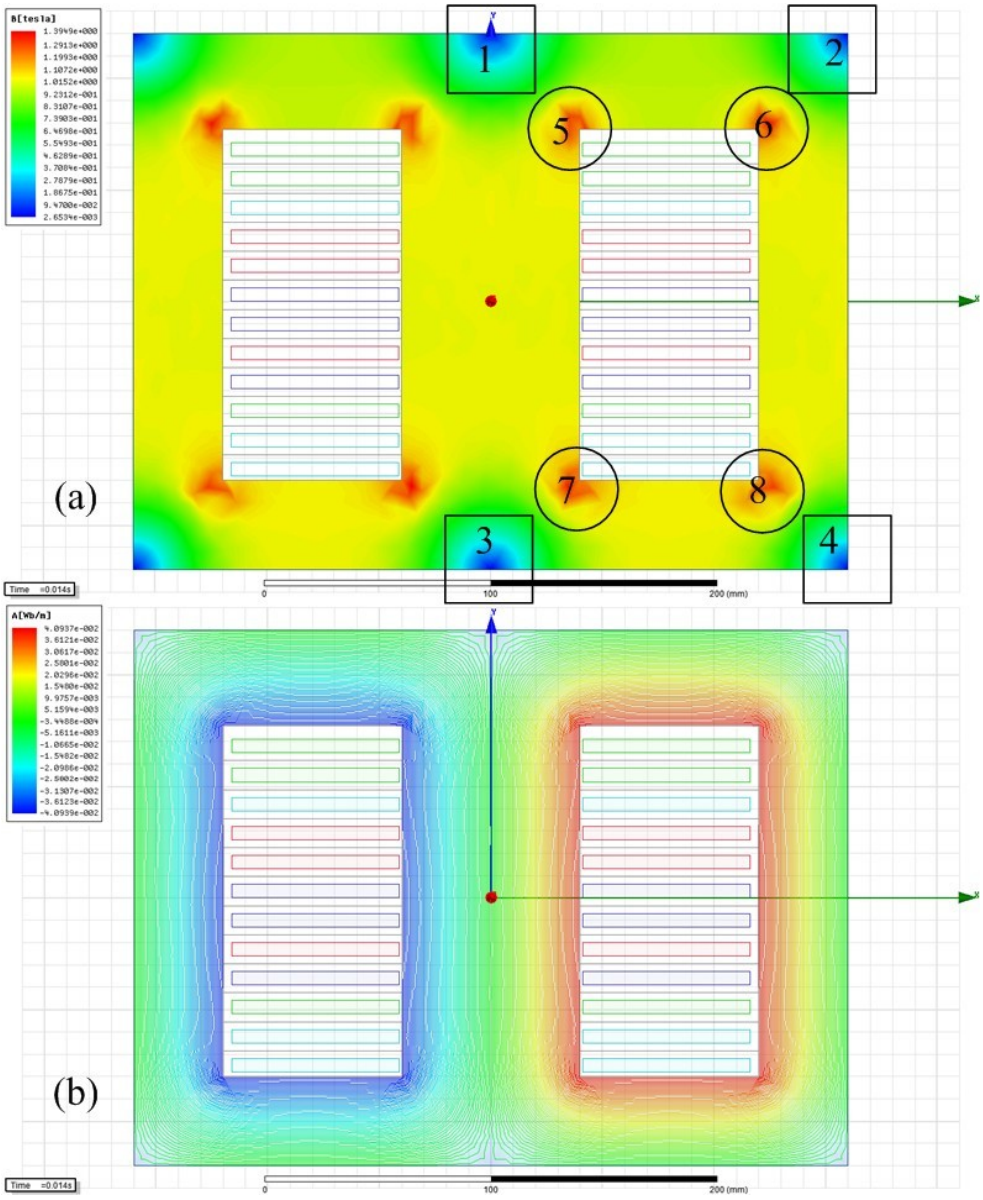

Figure 7 Schematic of lines and nodes position (see online version for colours)

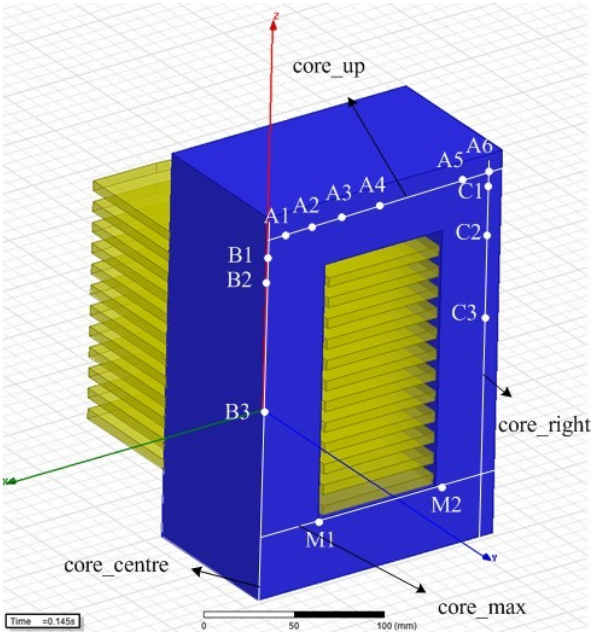

Figure 8 Mag_B distribution of nodes (see online version for colours)

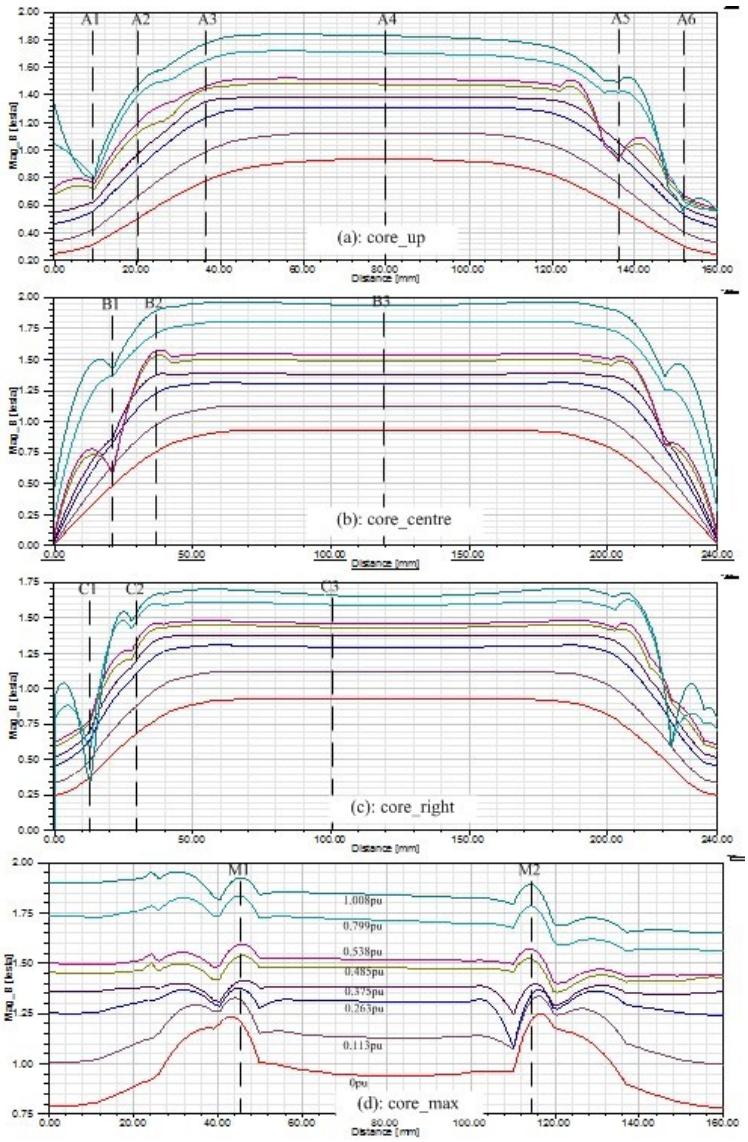

Figure 9 Mag_B of nodes Ai, Bi, Ci and Mi (see online version for colours)

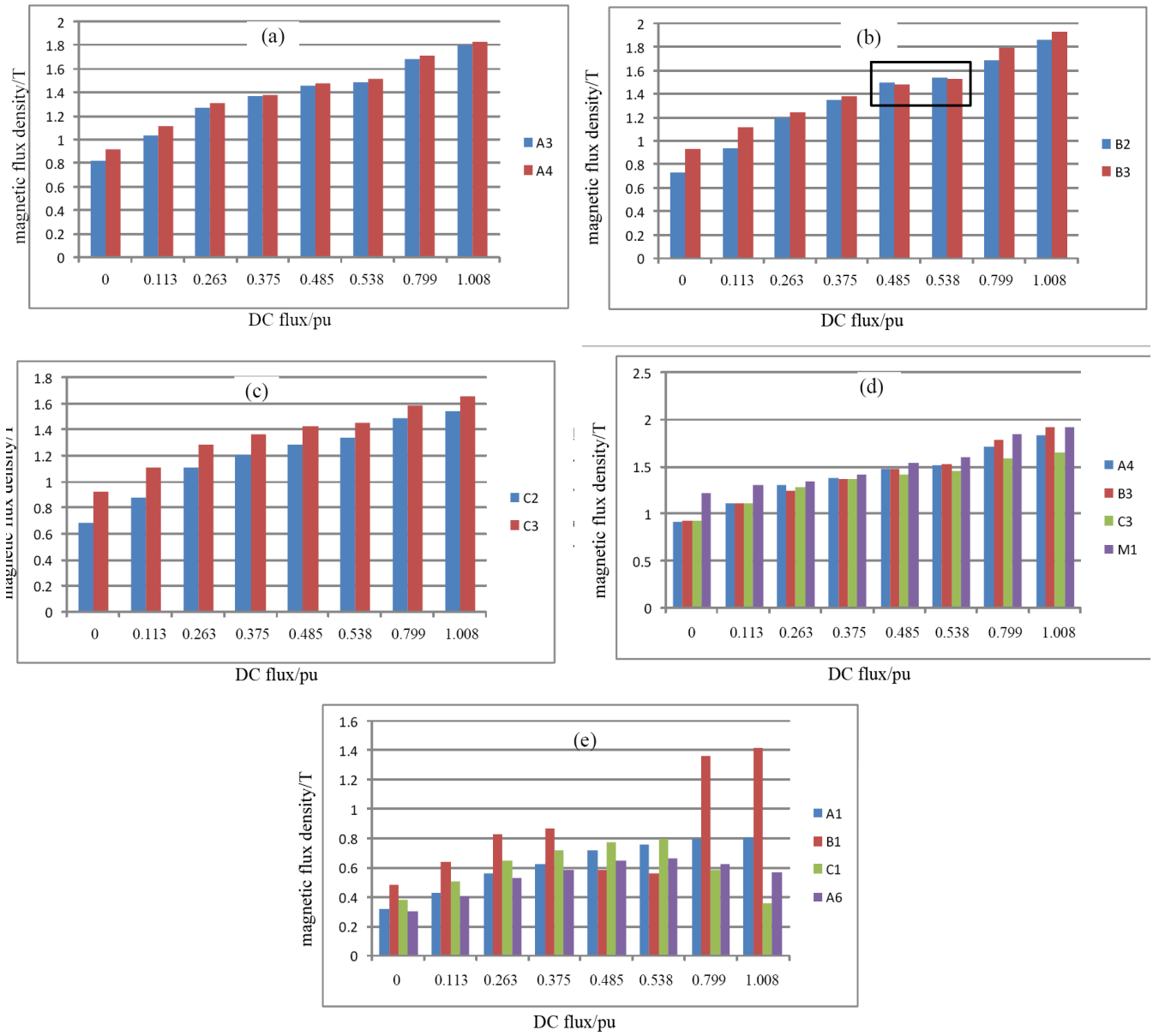

It has already been said in Figure 6, magnetic lines in rectangular box 1, 2, 3 and 4 are thinner than other parts. So Mag_B curves of 'core_up', 'core_centre' and 'core_right' look like trapezoids, that is to say Mag_B of two ends is larger and in the middle is smaller. In the same way, magnetic lines in the circle 5, 6, 7 and 8 are more intensive, and because they are near the corner of core window, Mag_B of point M1 and M2 in Figure 8(d) is the maximum in the whole core and there is a little distortion near them. In the middle of these curves, the lowest line means the DC flux is 0 pu and the highest means 1.008 pu. Figure 8(d) has labelled different DC flux at different Mag_B.

With the increasing of DC magnetic bias, Mag_B of most nodes is increasing either, such as point A2, A3 and A4 [in Figure 8(a)]; B2 and B3 [in Figure 8(b)]; C2 and C3 [in Figure 8(c)]; M1 and M2 [in Figure 8(d)]. And some other points have made a difference, such as A1, A5, A6, B1 and C1. Sometimes Mag_B at these nodes does not increase than decrease. For further analysis, Table A1 in the Appendix has recorded Mag_B value of every point marked in Figure 8.

Comparisons of Mag_B variation of A3 and A4, B2 and B3, C2 and C3 are shown in Figures 9(a) to 9(c). Take Figure 9(c) as an example, firstly the Mag_B of node C3 is always larger than node C2. Then, with the increasing DC magnetic bias, the difference between the Mag_B of node C2 and C3 is reducing gradually. It is easy get to know that the rising rate of Mag_B of node C2 is faster than node C3. The contrast between node A3 and A4 can get the same conclusion. Node A3 and C2 are in the region of rectangular box 1 and 2, node A4 and C3 are distributing in the middle of the centre column of core or the iron yoke. Figure 9(d) presents the histogram of Mag_B of A4, B3, C3 and M1. The first three nodes are all located in the middle of three lines in Figure 7. Node M1 and M2 are located in the maximum Mag_B position of which circle 5, 6, 7 and 8 in

Figure 6. From the histogram, the rising rate of Mag_B at the node M1 is the lowest, and then is node B3 and the fastest is node A4. So we can come to a conclusion that Mag_B of the centre column is always larger than which of the iron yoke, instead, the rising rate of Mag_B with DC flux of centre column of core is slower than the iron yoke.

Figure 9(e) chooses nodes A1, A6, B1 and C1 for comparison, which are all located at two edges and middle of iron yoke, and they are in the area of rounded rectangle 1, 2, 3 and 4 in Figure 6(a). It can be found that the DC flux is in the range of 0~0.375 pu, Mag_B of nodes above is rising with the increasing of DC magnetic bias. After the DC flux is larger than 0.375 pu, the Mag_B variation of these nodes is irregular. For instance, with the increasing of DC flux, the Mag_B of node A1 is still raising, which of C1 and B6 is decreasing and node B1 of which first increases then decreases. Node B2 in Figure 9(b) is also special; its Mag_B even becomes larger than point B2 as the DC flux is 0.485 pu. It is obvious that there are bumps near B2, M1 and M2, which is because these points are in the circle 5, 6, 7 and 8 in Figure 6(a), magnetic lines of these sections are so intensive that Mag_B curves are distorting. And those Mag_B variations of points in rounded rectangle 1, 2, 3 and 4 are in irregular change.

4.3 Leakage electromagnetic field

Two horizontal lines 'w_out' and 'w_in' are drawn in the middle of windings using the same methods in Section 4.2 in Figure 10, starting nodes are D1 and E1; finishing nodes are D5 and E4 respectively. Leakage Mag_B values of every node are recorded in the Appendix in Table A2 and Figure 11 show leakage Mag_B of these nodes

4.3.1 Horizontal comparison

Nodes from D1 to D5 of Mag_B are presented in Figure 11(a) and E1,…, E4 are shown in Figure 11(b). Figures 11(c) and 11(d) are partial enlarged detail of Figures 11(a) and 11(b) respectively. Among them, D1, …, D5 are located in the core window, D1 is situated the nearest of centre column and D5 is closing to the iron yoke right side; E1, …, E4 are located outside of the core, E1 is the nearest of the core and E4 is the farthest.

In Figure 11, with the rising of DC magnetic bias, leakage Mag_B is increasing. But the rising rate is different. That is because core saturation become more serious with the rising DC flux, the constraint capacity to magnetic lines will be weakened. So the leakage Mag_B gets larger.

According to Table A2 in the Appendix, Figure 12 presents variations of leakage Mag_B(mT) of nodes on line 'w_in' and 'w_out'. For Figures 12(a) and 12(c), variation of leakage Mag_B of each node is a little, but it is still a process of rising. DC magnetic bias increasing from 0 pu to 1.008 pu, the leakage Mag_B rising rate of node D1 is the fastest, D2, D3 and D5 take the second place and D4 is the slowest. It can be concluded that if the node located near the core, no matter the centre column or the iron yoke, the leakage Mag_B rising rate comes fastest. And Mag_B of centre column is larger than iron yoke on the basis of above analysis [see Figure 9(d)], and directions of B vector in the centre column and iron yoke are opposite, the extent of offset becomes greatest at node D4, so its variation rate is slowest.

Figure 10 Schematic of lines and nodes position (see online version for colours)

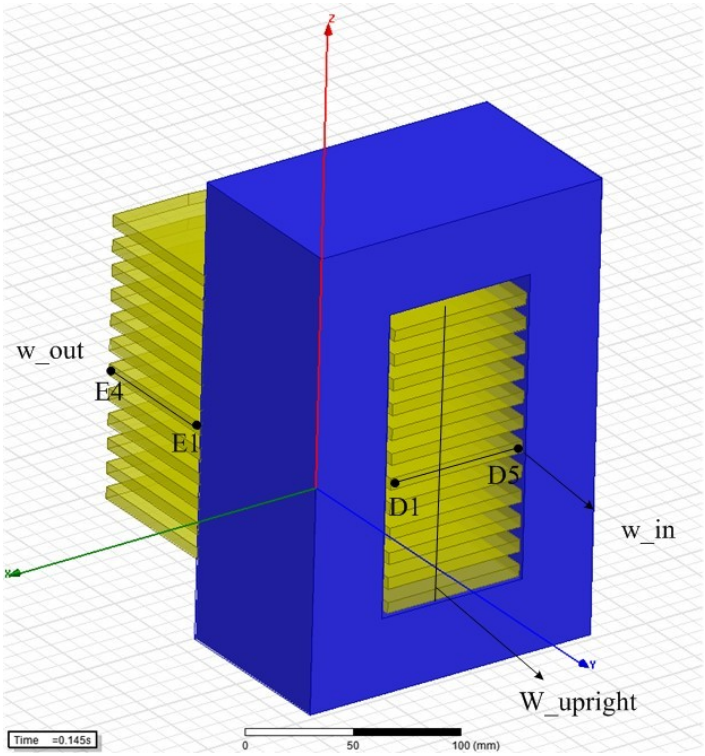

Figure 11 Mag_B distributions (see online version for colours)

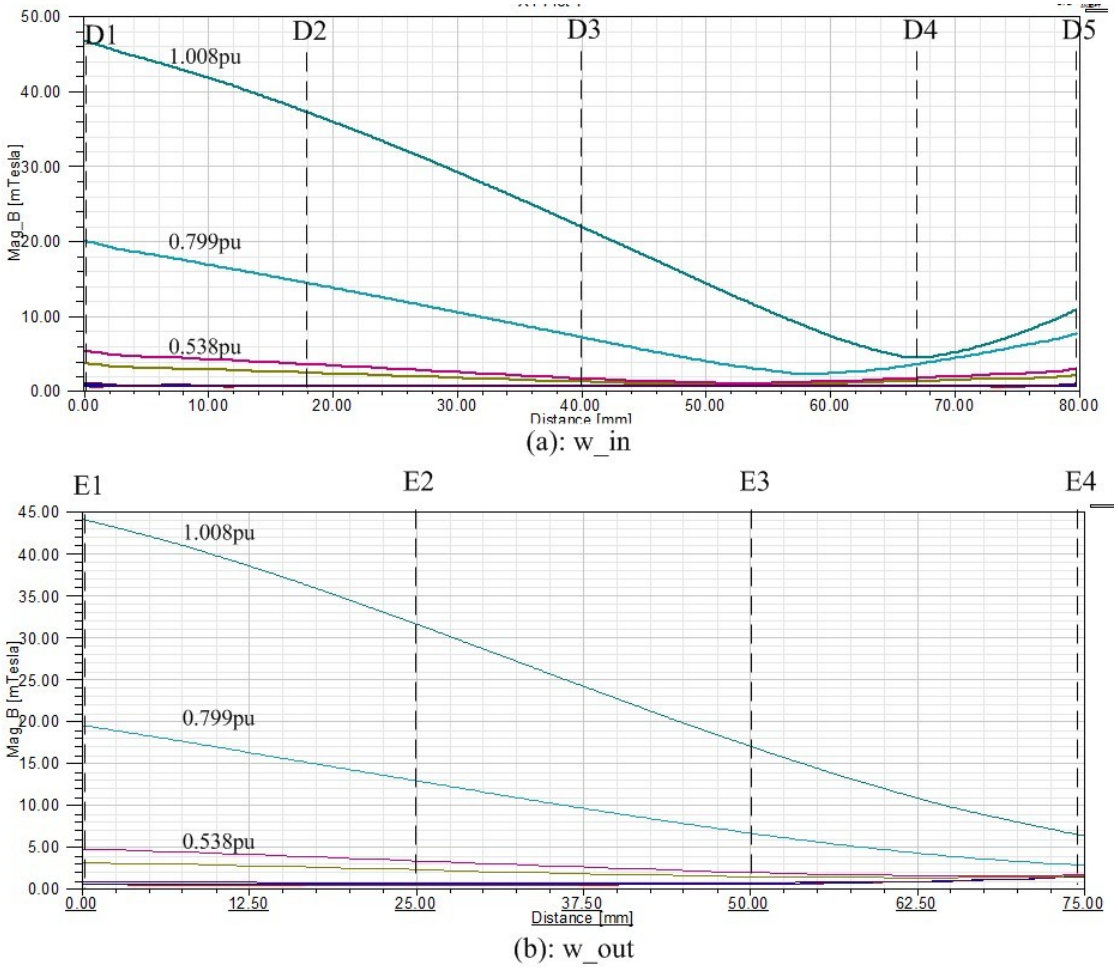

Figure 12 Histogram of Mag_B (see online version for colours)

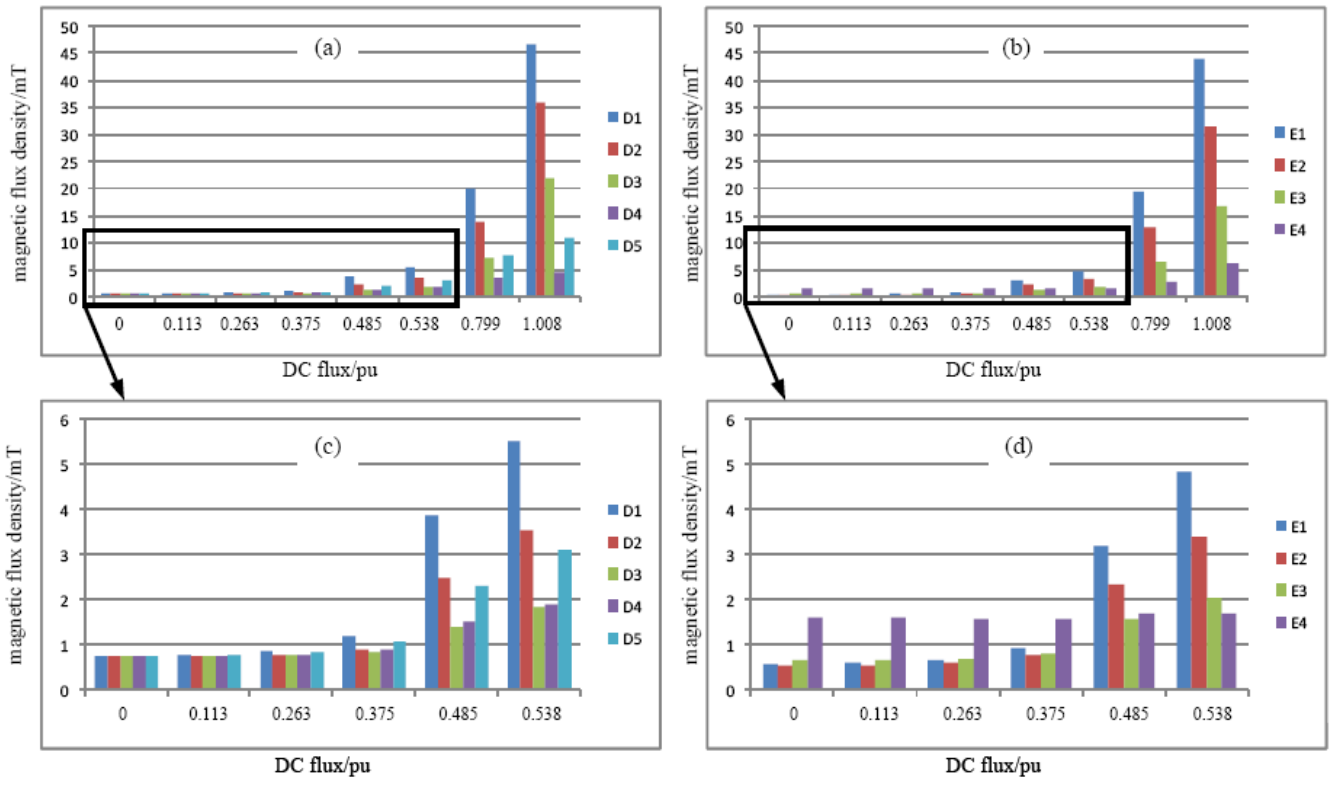

The variation rule is more simple relatively for Figures 12(b) and 12(d). As DC flux between 0 pu with 0.375 pu, the leakage Mag_B of node E4 far away from the core is larger than E1 that near the core. That is because the constraint capacity to magnetic lines is strong as the transformer works under normal circumstances or lightly saturation, so the leakage Mag_B is small relatively near the core. And core saturation will be serious with the continue rising of DC flux, the constraint capacity to magnetic lines will be weakened. So the leakage Mag_B has increased sharply. The Mag_B of E1 is increasing from 0.5806 mT to 44.1056 mT with the rising DC flux from 0 pu to 1.008 pu. Instead, the magnetic density of E4 almost does not change before the DC flux of 0.538 pu because it is far away from the core, and then it has a slight rising with the continue DC flux increasing. Longitudinal comparison.

A vertical line of 'w_upright' is drawn in the middle of windings. Some special nodes in the gap between windings have been picked out (see Figure 14). The leakage Mag_B values of every point are recorded in Table A2 in the Appendix as well.

According to the arrangement of interleaved windings, its magnetic potential distribution has been shown in Figure 13. The leakage Mag_B stays the same in gaps and linear change in windings. For adjacent windings, the variation trend of magnetic potential is the same as the current directions are the same.

Figure 14 presents leakage Mag_B variation of line 'w_upright' as DC flux of 0 pu, 0.375 pu and 1.008 pu. It can be seen that Figure 14(a) is consistent with Figure 13. But along with the DC magnetic bias rising, both ends of the curve have been greatly increased. According to the value record of Table A2 in Appendix, the Mag_B variation rules can be draw as Figure 15 and they are almost the same as variation rules of Figure 12. It could be simply summed up as that the rising rate of leakage Mag_B of nodes near the iron yoke is the fastest. Furthermore, the rising rate slowly increases as the little DC flux and fast increases as the larger DC flux.

Figure 13 Principle diagram of leakage Mag_B

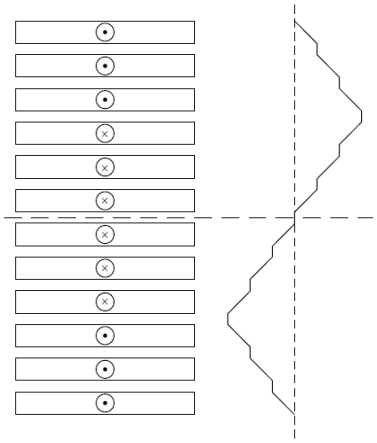

Figure 14 Leakage Mag_B of line 'w_upright' (see online version for colours)

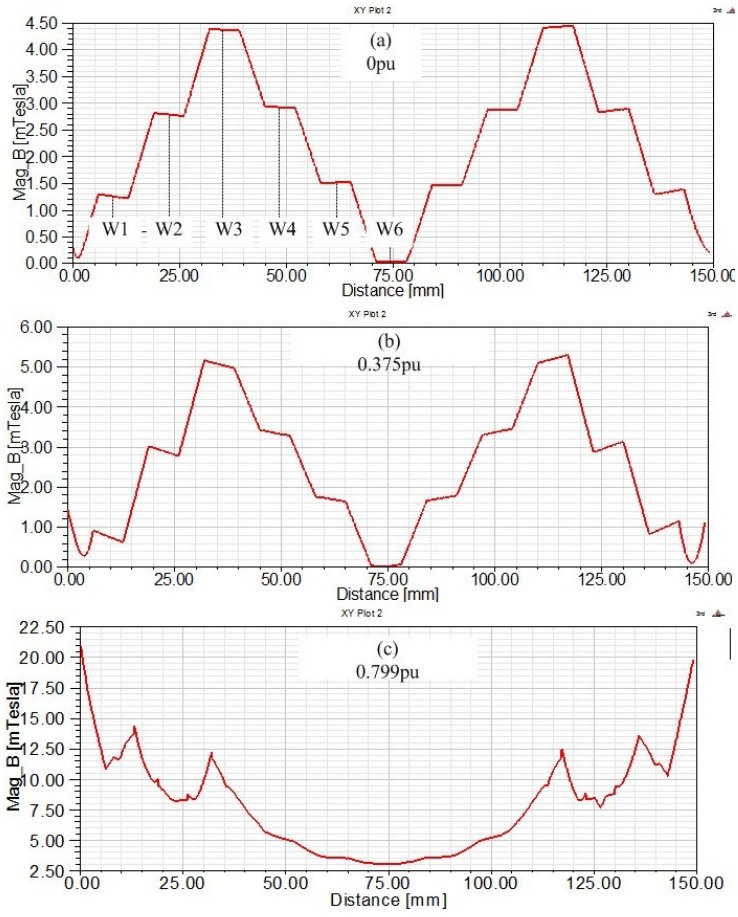

Figure 15 Histogram of Mag_B (see online version for colours)

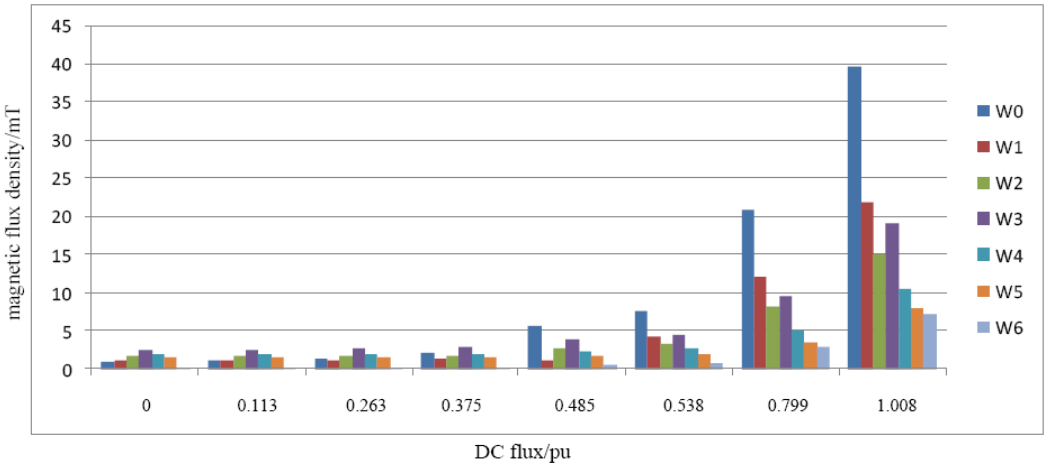

Variations of leakage Mag_B in windings, gaps and Mag_B in core are different. As the little DC flux, the leakage Mag_B almost stays the same but the Mag_B of core is increasing linearly; on the contrary, as the saturation intensified with the larger DC magnetic bias, the Mag_B rising rate of core becomes slow and the leakage Mag_B of windings and gaps get to great rising.

4.4 Leakage energy and leakage inductance

When transformer works under normal circumstances, no matter input voltage or load current, they would not change suddenly, and leakage flux and current are in a linear relationship. From Figure 5, primary current has distorted to spire waveforms and the amplitude increases sharply as a larger DC flux [see Figure 16(a)]. Secondary current is still sinusoidal waveform because DC component could not transfer to secondary windings. At the same time, core saturation will weaken the constraint capacity to magnetic lines, which will as well as lead to the rising leakage Mag_B. So the leakage magnetic field energy almost raises exponential [see Figure 16(b)]. Under the combined action of current and leakage magnetic field energy, variation rules of leakage inductance could be concluded. With the rising of DC magnetic bias, secondary leakage inductance will increase and primary leakage inductance will decrease [see Figure 16(c)]. All these parameters of transformer are not changing linearly. Variations are not obvious as DC bias is small and increasing significantly with the larger DC flux. Although a great DC bias, the primary leakage inductance does not change too much because both sharp variation of the primary current and primary leakage magnetic field energy. The exponential variation of secondary leakage inductance because of the invariant secondary current and the sharp increasing leakage magnetic field energy.

5 Conclusions

This paper has set up the coupled finite element model of PCS and coupled field-circuit model of the main transformer. Regard the disconnection rules as the control signal of the external circuit of transformer, the frequent disconnection will lead to DC magnetic bias of transformer. And this paper also study variations of Mag_B and variations of leakage inductance caused by DC magnetic bias. Some conclusions have been shown the following.

With the increasing of DC flux, primary current, leakage magnetic field energy, and Mag_B in and out of core are all rising. When the DC magnetic bias is little relatively, Mag_B of core lineally raises and leakage Mag_B, primary current and leakage magnetic field energy slowly increase. Instead, when the DC magnetic bias get larger, the rising rate of Mag_B of core slow down, at the same time, leakage Mag_B, primary current and leakage magnetic field energy raises almost exponential.

About the variation situation of Mag_B, with the rising of DC flux, the magnetic density of centre column of core is larger than iron yoke, but the maximum position of Mag_B is near the corner of core window. The Mag_B variation rules of both ends and the middle of iron yoke are irregular such as first increase then decrease. For the leakage magnetic features, leakage Mag_B of some nodes far away from the core is larger than other points around the core due to a little DC bias. After the DC bias raises fast, leakage Mag_B of remote positions of core increase slowly but positions nearby sharply raise, so its value will larger than the former. The increase of leakage magnetic field energy is also because of this.

For the leakage inductance, with the rising of DC bias, secondary leakage inductance will increase and primary leakage inductance will decrease. In the same way, when the DC bias is little, variations of two parameters are not obvious. With continue rising of DC bias, the secondary leakage inductance sharply increasing and the primary leakage inductance falling slowly.

Table 4 Leakage energy and leakage inductance

	DC flux/pu	*0*	*0.113*	*0.263*	*0.375*	*0.485*	*0.538*	*0.799*	*1.008*
Current/pu	Primary1	1.0010	1.0086	1.0108	1.0131	1.0142	1.0452	1.162	1.3325
	Primary2	1.0011	1.0021	1.006	1.0077	1.0086	1.03	1.1213	1.3307
	Secondary1	1.0032	1.003	1.0025	1.0023	1.0021	1.002	0.9987	0.9904
	Secondary2	1.0022	1.0026	1.0028	1.003	1.0031	1.003	1.0011	1.0013
Leakage energy/J	Primary1	0.0848	0.0849	0.085	0.0851	0.0852	0.0866	0.09	0.1166
	Primary2	0.0848	0.0849	0.085	0.0851	0.0851	0.0865	0.0895	0.1157
	Secondary1	0.1032	0.1033	0.1034	0.1036	0.1036	0.1047	0.1076	0.1415
	Secondary2	0.0676	0.0677	0.0677	0.0678	0.0678	0.0684	0.0708	0.0959
Leakage inductance/mH	Primary1	0.5973	0.5952	0.5933	0.5913	0.5904	0.5652	0.4752	0.4678
	Primary2	0.6021	0.6004	0.5989	0.5974	0.5967	0.5815	0.5075	0.4659
	Secondary1	0.7288	0.731	0.7329	0.7348	0.7357	0.7484	0.7819	1.0538
	Secondary2	0.4797	0.4798	0.4799	0.4801	0.4802	0.4878	0.5036	0.6816

Figure 16 Features of leakage inductance (see online version for colours)

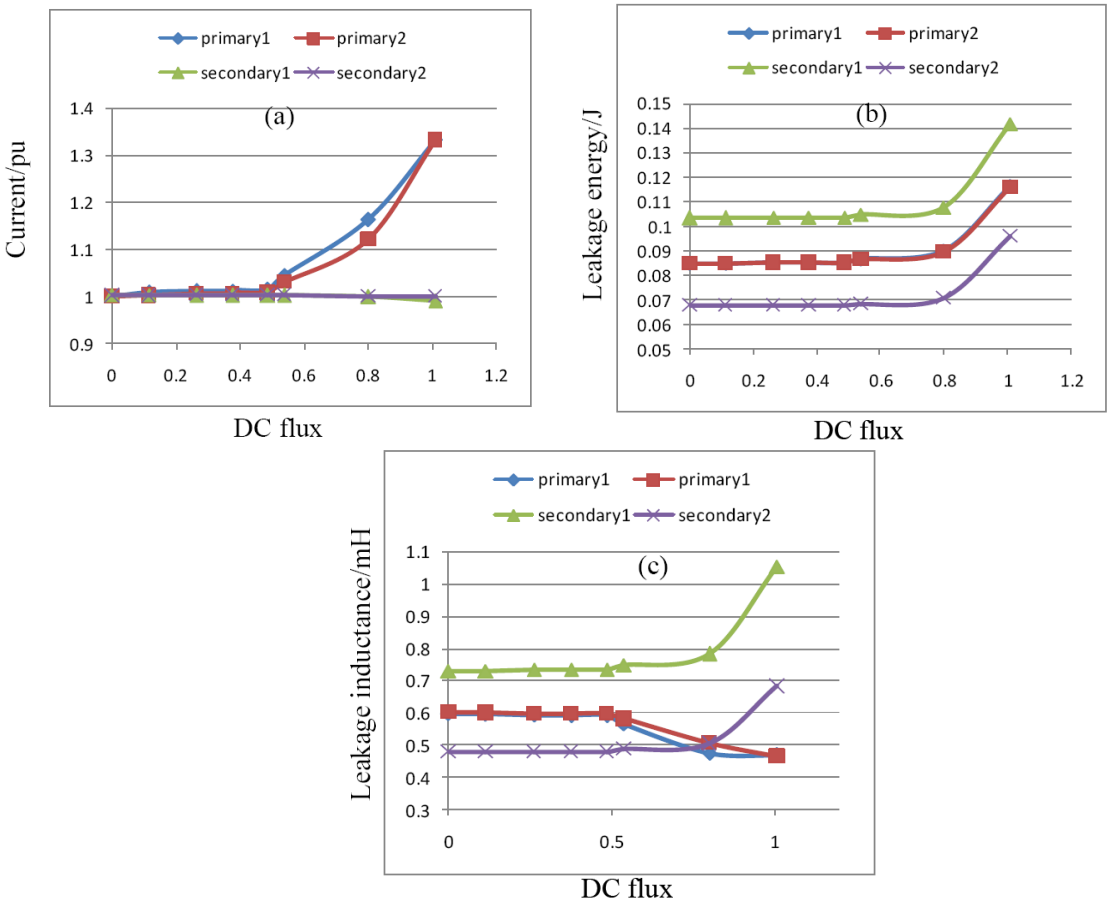

During high-speed train operation, frequent disconnection will affect the quality of current collection of the main transformer, and then impact on its output and electromagnetic features. Effects of high-frequency contact loss of PCS reflect on DC component of primary current, harmonic, grid-side power factor, torque pulsation and even the stability of the traction drive system, especially during braking operations, energy feedback of the main transformer would be affected by high-frequency disconnection, and then the stability of the braking system even the safe operation of high-speed train would also be affected. Therefore, follow-up studies of this paper will towards this direction. And a whole simulation model consists of PCS including dynamic model and mathematical model of pantograph arc, traction drive system model of the main transformer, traction converter and traction motor will be set up in the future for further research. Above all analysis of effects on the main transformer cause by high-

frequency disconnection will provide the basis for analysis effects on traction drive system during the operation of high-speed train.

Acknowledgements

This work was supported by a grant from the Major State Basic Research Development Programme of China (973 Programme: 2011CB711100).

References

Bucca, G., Collina, A., Manigrasso, R., Mapelli, F. and Tarsita, D. (2011) 'Analysis of electrical interferences related to the current collection quality in pantograph-catenary interaction', in *Proceedings of the Institution of Mechanical Engineers, Part F: Journal of Rail and Rapid Transit*, 19 August, p.483.

Chan, Y.P. and Pong, M.H. (2006) 'Leakage inductance calculation of complex transformer constructions based on a simple two-coil inductor model', *IEEE PESC '06*, pp.1–4.

Collina, A. and Bruni, S. (2002) 'Numerical simulation of pantograph-overhead equipment interaction', *Vehicle System Dynamics*, Vol. 38, No. 31, pp.261–291.

Frank, W.D. (1995) 'Torque ripple considerations on large (mill) drives in the cement industry', in *Proc. IEEE XXXVII Cement Ind. Tech. Conf.*, pp.411–432.

Hedayati, K.S., Fabio, B., Augustinet, M-M. et al. (2010) 'Pantograph-catenary interaction model comparison', in *36th Annual Conference of the IEEE Industrial Electronics Society*, pp.1584–1589.

Heinemann, L. and Helfrich, J. (2000) 'Modeling and accurate determination of winding losses of high frequency transformers in various power electronics applications', *IEEE APEC '00*, Vol. 2, pp.647–653.

Jianshe, W. (1996) 'A nodal analysis for 2D and 3D magnetic-circuit coupled problems', *IEEE Trans. on Magnetics*, Vol. 32, No. 3, pp.1074–1077.

Lee, K., Jahns, T.M., Berkopec, W.E. and Lipo, T.A. (2006) 'Closed-form analysis of adjustable-speed drive performance under input-voltage unbalance and sag conditions', *IEEE Transactions on Industry Applications*, Vol. 42, No. 3, pp.733–741.

Li, P., Huang, G., Xie, L. and Hu, X. (2008) 'Research on calculating leakage inductance of power transformer and its application to winding deformation analysis', *CICED2008 Technical Session 1 Distribution Network Equipment*, pp.1–6.

Liu, R., Liu, W., Yang, H., Gong, Z. and Wang, W. (2011a) 'Simulation of dynamic current collection between pantograph and catenary of elastic catenary suspension system', in *Proceedings of the 1st International Workshop on High-Speed and Intercity Railways*, Vol. 1 pp.489–494, 19–22 July, Hong Kong, China.

Liu, W., Yang, Z., Gong, Z., Wang, W., Yang, H. and Liu, R. (2011b) 'A study on the generated characteristics of the arc discharge for contact-loss of pantograph', in *Proceedings of the 1st International Workshop on High-Speed and Intercity Railways*, Vol. 2, pp.1–7, 19–22 July, Hong Kong, China.

Manabe, K. (1992) 'Catenary-pantograph system for speed up of Shinkansen train', *Japanese Railway Engineering*, Vol. 11, No. 7, pp.10–13.

Manabe, K., Morikawa, T. and Hikata, M. (1986) *On Dynamics of Overhead Equipment and Multi-pantograph System*, pp.21–25, Quarterly Reports of RTRI.

Mei, G., Liu, Y. and Guo, M. (2008) 'Study of transformer's harmonic characteristic in DC magnetic bias', in *Electricity Distribution, CICED, China International Conference*, pp.1–4.

Nystrom, A., Hylander, J. and Thorborg, K. (1988) 'Harmonic currents and torque pulsations with pulse width modulation methods in AC motor drives', in *Proc. 3rd Int. Conf. Power Electron, Adjustable-Speed Drives*, pp.378–381.

Piriou, F and Razak A. (1998) 'A non-linear coupled 3D model for magnetic field and electric circuit equations', *IEEE Trans. on Magnetics*, Vol. 28, No. 2, pp.1295–1298.

Robert, F. and Meshal, R. (2000) 'Dynamic interaction between pantograph and overhead track equipment for heavy haul operations', *Vehicle System Dynamics*, Vol. 33, No. S, pp.478–489.

Seo, J-H., Jung, I-H. and Park, T-W. (2005) 'Dynamic analysis of a multibody system including a very flexible beam element', *JSME International Journal, Series C: Mechanical Systems, Machine Elements and Manufacturing*, Vol. 48, No. 2, pp.224–233.

Siti, R.M., Hassan, S. and Anuar, M.N K. (2012) 'Study the harmonic characteristics of DC bias on the single phase power transformer', in *Power Engineering and Optimization Conference (PEDCO), IEEE International*, pp.501–501, Melaka, Malaysia.

Spangler, J.J. (2002) 'A low cost, simple torque ripple reduction technique for three phase inductor motors', in *Proc. IEEE APEC*, Vol. 2, pp.759–763.

Tang, R.Y., Wang, S.H. and Li, Y. (2000) 'Transient simulation of power transformers using 3D finite of power transformers using 3D finite element model coupled to electric circuit equations', *IEEE Trans on Magnetics*, Vol. 36, No. 4, pp.1417–1420.

Tibor, G., Catalin, B., Yoshihiro, S. et al. (1997) 'Simulation of electric drive system of electric rolling stocks', in *Proceedings of the 1997 International Conference on Intelligent Engineering Systems*, pp.365–370.

Vinayagalingam, T. (1983) 'Computer evaluation of controlled pantographs for current collection from simple catenary overhead equipment at high speed', *ASME Journal of Dynamic Systems, Measurement, and Control*, Vol. 105, No. 4, pp.287–294.

Wang, J., Witulski, A.F., Vollin, J.L., Phelps, T.K. and Cardwell, G.I. (1999) 'Derivation, calculation and measurement of parameters for a multiwinding transformer electrical model', *IEEE APEC '99*, Vol. 1, pp.220–226.

Xuejun, M. and Dan, Z. (2010) 'Computation of leakage flux and magnetic force in transformer by using field-circuit coupled finite element method', in *Power and Energy Engineering Conference (APPEEC)*, pp.1–4, Asia-Pacific.

Zeng, L., Zhu, Z., Bai, B. and Song, Y. (2007) 'Research on influence of DC magnetic bias on a converter transformer', in *Electrical Machines and Systems, ICEMS, International Conference*, pp.1346–1349.

Appendix

Table A1 Mag_B(T) of nodes

Line	*DC flux/pu*	*0*	*0.113*	*0.263*	*0.375*	*0.485*	*0.538*	*0.799*	*1.008*
Core_up	A1	0.3237	0.4281	0.5608	0.6281	0.7213	0.7594	0.7972	0.8042
	A2	0.5102	0.6694	0.8707	0.9752	1.1256	1.2034	1.3979	1.4737
	A3	0.8207	1.0357	1.2709	1.3712	1.4593	1.4948	1.6845	1.8069
	A4	0.9204	1.1210	1.3093	1.3817	1.4779	1.5198	1.7164	1.8372
	A5	0.5823	0.7577	0.9673	1.0545	0.9454	0.9316	1.4189	1.4912
	A6	0.3061	0.4063	0.5328	0.5906	0.6498	0.6704	0.6310	0.5760
Core_centre	B1	0.4881	0.6424	0.8297	0.8691	0.5885	0.5681	1.3627	1.4177
	B2	0.7306	0.9418	1.1983	1.3529	1.4993	1.5337	1.6793	1.8639
	B3	0.9277	1.1175	1.2476	1.3775	1.4803	1.5306	1.7927	1.9292
Core_right	C1	0.3849	0.5061	0.6546	0.7198	0.7789	0.7979	0.5901	0.3596
	C2	0.6885	0.8853	1.1119	1.2106	1.2847	1.3405	1.4901	1.5415
	C3	0.9256	1.1147	1.2922	1.3673	1.4274	1.4563	1.5891	1.6549
Core_max	M1	1.2214	1.3153	1.3525	1.4230	1.5469	1.6069	1.8448	1.9291
	M2	1.2293	1.3112	1.3470	1.4283	1.5415	1.5932	1.8012	1.8997

Table A2 Mag_B(mT) of nodes

W_in	D1	0.7554	0.7855	0.8720	1.2132	3.8854	5.5307	20.1633	46.7497
	D2	0.7600	0.7670	0.7880	0.9136	2.5012	3.5715	13.8789	35.9430
	D3	0.7688	0.7794	0.7993	0.8499	1.4143	1.8405	7.2730	21.9408
	D4	0.7613	0.7699	0.8026	0.9051	1.5171	1.9237	3.7983	4.5956
	D5	0.7595	0.7869	0.8650	1.0891	2.3217	3.1230	7.7986	11.0524
W_out	E1	0.5806	0.6081	0.6625	0.9311	3.2123	4.8522	19.5717	44.1065
	E2	0.5451	0.5659	0.6096	0.8052	2.3478	3.4250	12.9440	31.5754
	E3	0.6634	0.6778	0.7065	0.8248	1.5842	2.0683	6.7168	17.0170
	E4	1.6108	1.6072	1.5948	1.5940	1.6985	1.7181	2.9031	6.4694
W_upright	W0	1.0437	1.1644	1.4663	2.1736	5.7087	7.6463	20.9237	39.7550
	W1	1.0877	1.0963	1.1453	1.3805	1.2573	4.3897	12.0585	21.9296
	W2	1.7066	1.7116	1.7256	1.8207	2.7622	3.4097	8.2688	15.1101
	W3	2.5902	2.6192	2.6806	2.8561	3.9094	4.5367	9.6201	19.1982
	W4	1.9011	1.9078	1.9180	1.9738	2.3908	2.6515	5.0989	10.6556
	W5	1.5017	1.5020	1.4984	1.5213	1.7491	1.8982	3.5505	7.9934
	W6	0.0320	0.0355	0.0443	0.0183	0.5344	0.8472	3.0213	7.2220